Vol. 90 No. 1 pp. 121–137 ACTA GEOLOGICA SINICA (English Edition) Feb. 2016

Geochemistry and Genesis of Iron-apatite Ore in the Khanlogh Deposit, Eastern Cenozoic Quchan-Sabzevar Magmatic Arc, NE Iran

Arezo ZAREI, Azadeh Malekzadeh SHAFAROUDI* and Mohammad Hassan KARIMPOUR

Research Center for Ore Deposit of Eastern Iran, Ferdowsi University of Mashhad, P.O. Box 91775-1436, Mashhad, Iran

Abstract: The Khanlogh deposit in the Cenozoic Quchan-Sabzevar magmatic belt, NE Iran, is hosted by Oligocene granodioritic rock. The Khanlogh intrusive body is I-type granitoid of the calc-alkaline series. The orebodies are vein, veinlet, massive, and breccia in shape and occur along the fault zones and fractures within the host rock. Ore minerals dominantly comprise magnetite and apatite associated with epidote, clinopyroxene, calcite, quartz, and chlorite. Apatites of the Khanlogh deposit have a high concentration of REE, and show a strong LREE/HREE ratio with a pronounced negative Eu anomaly. Magnetites have a high concentration of REE and show weak to moderate LREE/HREE fractionation. They are comparable to the REE patterns in Kiruna-type iron ores and show an affinity to calc-alkaline magmas. The Khanlogh deposit is similar in the aspects of host rock lithology, alteration, mineralogy, and mineral chemistry to the Kiruna-type deposits. Field observations, hydrothermal alteration halos, style of mineralization, and the geochemical characteristics of apatite, magnetite, and host rock indicate that these magnetite veins have hydrothermal origin similar to Cenozoic Kiruna-type deposits within the Tarom subzone, NW Iran, and are not related to silica-iron oxide immiscibility, as are the major Precambrian magnetite deposits in central Iran.

Key words: Trace and rare earth elements, iron oxide-apatite, Kiruna-type, Quchan-Sabzevar magmatic arc, Khanlogh, Iran

1 Introduction

Trace elements and REE distributions in apatite and magnetite of different ore types show characteristic patterns that are related to different modes of formation of the ores. The rare earth elements are fractionated by petrological and mineralogical processes. The REE content of igneous minerals is controlled by the mineral-melt distribution coefficients and REE patterns depend on the bulk REE composition of the parent magma (Taylor and McLennan, 1985). Apatites contain REE in small amounts replacing Ca^{2+} and play an important role for the REE distribution in ores and rocks (Hughes et al., 1991). Many studies also indicate that apatite may also contain significant amounts of Sr, U, Y, Mn, and Th (Watson and Green, 1981; Dawson et al., 1996; Belousova et al., 2002; O'Reilly and Griffin, 2002; Dawson and Hinton, 2003). There is sparse knowledge of the distribution and content of REE in magnetite in different rock and ore types, whereas content of trace elements has been the subject of research studies for ten years (Carew, 2004; Carew et al., 2006; Singoyi et al., 2006; Beaudoin and Dupuis, 2009; Rusk et al., 2009; Dupuis and Beaudoin, 2011; Zhang et al., 2011; Berzina, 2012; Nadoll et al., 2012; Xiaowen et al., 2014). Of crucial importance is the similarity between the REE patterns in apatite, magnetite and the igneous host rock, pointing to consanguinity between them.

Iron oxide-apatite deposits can be divided into two major groups: 1) high-Ti, apatite-rich magnetite-ilmenite deposits (nelsonites) associated with anorthosites, and 2) low-Ti magnetite deposits with variable amounts of apatite (Kiruna-type), principally associated with calc-alkaline to alkaline volcanic rocks (Hildebrand, 1986; Frietsch and Perdahl, 1995). Kiruna-type iron oxide-apatite deposits and iron oxide copper-gold (IOCG) style deposits are considered end members of a continuum of mineralized systems (Hitzman et al., 1992; Hitzman, 2000; Gelcich et al., 2005). These deposits developed in the post-Archaean tectonic regimes in areas typified by igneous activity (Hitzman, 2000). Williams et al. (2005) and Williams (2010) consider that Kiruna-type deposits cannot be categorized as IOCG deposits and hence refer to them as

* Corresponding author. E-mail: shafaroudi@um.ac.ir

'IOA' (Williams, 2010), or P-rich iron oxide deposits (Groves et al., 2010).

Many IOA deposits, including world-class Chogart, Chador Malu, and Esfordi deposits, have been discovered in the Bafq district of Central Iran (Posht-e-Badam Block) (e.g. Forster and Jafarzadeh, 1994; Daliran, 2002; Daliran et al., 2007, 2010; Jami et al., 2007; Bonyadi et al., 2011; Mokhtari et al., 2013) (Fig. 1). The ore bodies of Posht-e-Badam Block are hosted by a lower Cambrian volcano-sedimentary sequence (also known as Saghand Formation) composed of lavas, pyroclastic, epiclesis rocks, intercalated carbonates, associated with number of mafic and felsic intrusions (Jami, 2005; Torab and Lehmann, 2007). The REE patterns of apatites in different deposits of Posht-e-Badam Block iron-apatite ores show an affinity to alkaline to sub-alkaline magmas and rifting environment. These ores have formed during magmatism as immiscible liquids (silicate and Fe-P-rich magmatic liquids), which separated from strongly differentiated magmas aided by a large volatile and alkali element content (Mokhtari et al., 2013). Also, a number of IOA deposits occur within the Tarom subzone of Alborz-

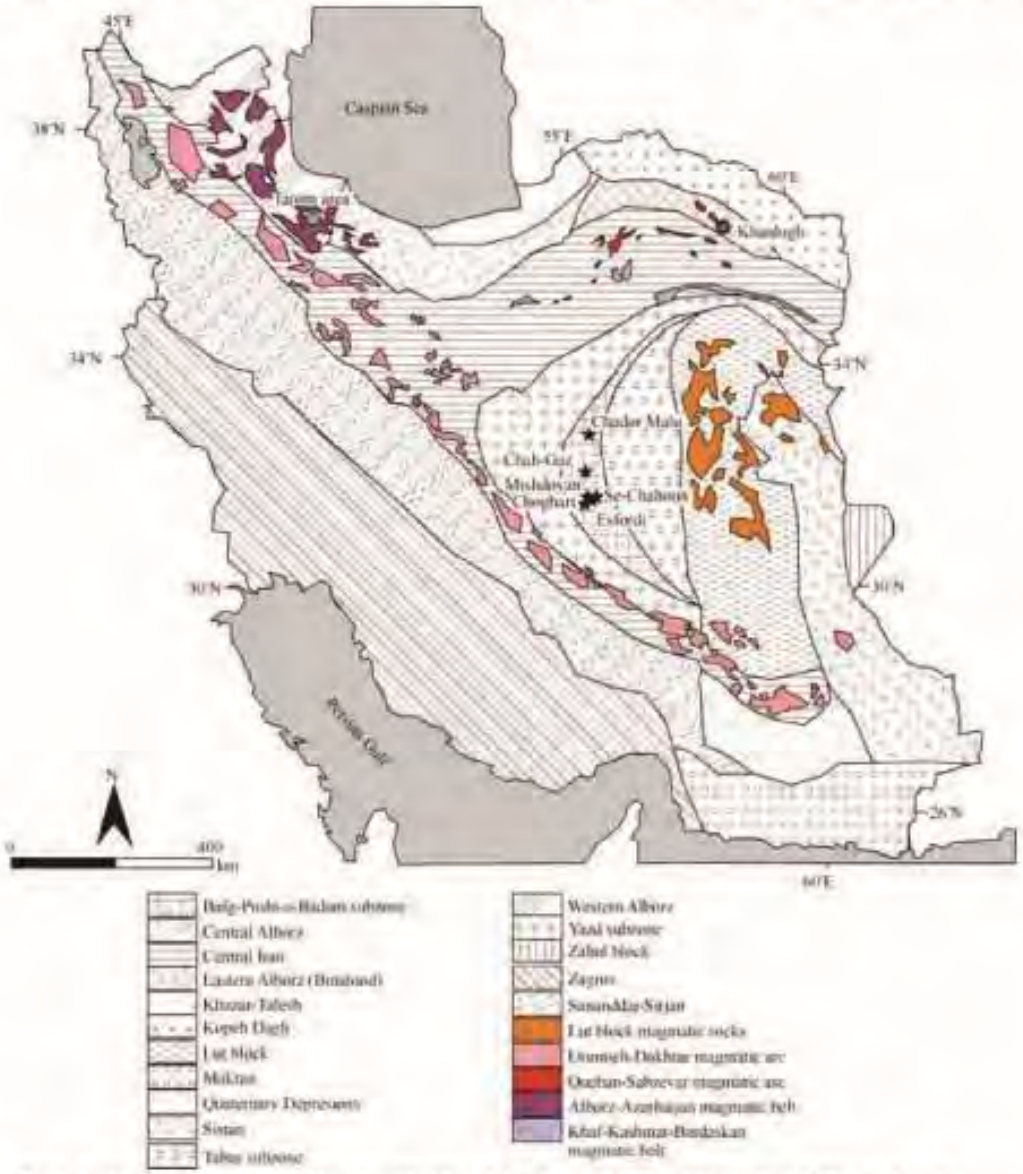

Fig. 1. Geological-structural map of Iran (modified from Sahandi et al., 2002) and the location of IOA ore deposits.

Azarbaijan volcano-plutonic structural zone, NW Iran (Fig. 1). The major deposits are at Sorkhe-Dizaj, Aliabad, Morvarid, and Zaker. These deposits are hosted mainly by post-Eocene–Early-Oligocene plutonic rocks and locally by Eocene volcanic-volcanoclastic rocks. They are related to calc-alkaline magmas generated in an active continental margin geodynamic environment. The geological studies, mineralogy and hydrothermal alteration suggest magmatic-hydrothermal origin for these deposits (Azizi et al., 2009; Nabatian et al., 2012; Nabatian and Ghaderi, 2013).

Recent exploration has led to the discovery of a low tonnage IOA deposit in the Cenozoic Quchan-Sabzevar magmatic arc, NE Iran (Fig. 1). Khanlogh is a first IOA occurrence of the NE Iran located 25 km northwest of Nyshabour. The mineralogy, alteration, and ore texture of deposit are studied by Zarei et al. (2014) and it is considered as Kiruna-type deposit. This paper presents an investigation on the geochemistry of trace and rare earth elements in the apatite, magnetite, and host rock in the Khanlogh deposit, their genetic relation, and genesis of iron-apatite ore.

2 Geological Setting

The Khanlogh IOA deposit occurs within the NW-trending Cenozoic Quchan-Sabzevar magmatic arc, NE Iran (Fig. 1). In this volcanic-plutonic belt, magmatic activities started since the Eocene (about 40 Ma ago) and continued to Plio-Pleistocene (about 2 Ma ago) (Spies et al., 1984). The volcanic and plutonic rocks of the arc can be divided in three groups (Spies et al., 1984): Eocene intermediate igneous rocks, Oligocene-Pliocene acidic igneous rocks, and Miocene-Pleistocene alkaline rocks (alkaline basalts and shoshonites). The first two groups (acidic to intermediate plutonic and volcanic rocks) are metaluminous to peraluminous and medium-K calc-alkaline, whereas the third and smallest group (alkaline rocks) is metaluminous and high-K to shoshonitic, with being generated in an active continental margin geotectonic environment (Spies et al., 1984). The calc-alkaline volcanism was generated by partial melting of the mantle wedge above a northwardly directed subduction zone between Sabzevar Neo-Tethyan oceanic lithosphere and the continental margin of the Turan plate (Spies et al., 1984). Baumann et al. (1983) presented initial $^{87}Sr/^{86}Sr$ ratios of Cenozoic post-ophiolitic calc-alkaline and alkaline igneous rocks range between 0.7035 and 0.7060, with a maximum between 0.7040 and 0.7052 (average 0.7046). They suggested this magmatism have been generated by dehydration of an oceanic crust and by partial melting of the mantle wedge above a subduction zone without contribution of sialic continental crust. They believed the variations in Sr isotopic composition may due to mantle heterogeneity and to various degrees of fractional crystallization, which is playing a dominant role in the formation of calc-alkaline magmas (Baumann et al., 1983).

The Quchan-Sabzevar Cenozoic magmatic arc has great potential for discovery of different types of mineralization, such as porphyry copper, epithermal copper, iron-oxide copper-gold (IOCG), and Fe-oxide deposits. However, little is known about the ore metal potential of this arc. The Neyshabour Turquoise mine as Cu-Au-U-LREE IOCG type mineralization (Karimpour et al., 2012), Jalambadan porphyry Cu-Au (Fatehi, 2014), Shotorsang magnetite (Gholami, 2009), Khanlogh Kiruna-type (in this study), and several Fe and Cu occurrences are related to this Cenozoic magmatic activity in northeast of Iran.

The geology of the Khanlogh deposit developed during the Cenozoic era (Fig. 2). The oldest rock in the study area is hornblende dacite (Fig. 2), which has been intruded by granodioritic units. Trace element distributions, petrographic and geochemical evidence suggest that the acidic rocks are of I-type granitoids of calc-alkaline, magmatic series (Malekzadeh Shafaroudi et al., 2014). The Eocene sedimentary rocks, including conglomerate and sandstone, are covered by the hornblende dacite with normal contact in some places of the region, and therefore the acidic subvolcanic and volcanic rocks are clearly post-Eocene in age. The geochronologic control is unavailable, but according to the geological map of Nyshabour (Ghaemi et al., 1998), these igneous rocks are related to Oligocene magmatism activity in the area. The hornblende dacite unit is light gray in color and porphyritic. This rock is composed of plagioclase (oligoclase), K-feldspar, hornblende, and quartz plus accessory magnetite. It is hydrothermally altered, without any magnetite-apatite mineralization. Epidote, chlorite, and calcite are main secondary minerals.

The granodioritic bodies are restricted between two thrust faults with approximately an east-west direction and consist of hornblende granodiorite porphyry and granodiorite porphyry as stock. The field study and mapping have shown that the magnetite-apatite veins are hosted by hornblende granodiorite porphyry (Fig. 2). These subvolcanic rocks are porphyritic with medium to coarse grained groundmass and plagioclase (oligoclase-andesine), orthoclase, and quartz are the main minerals. In addition, hornblende (4vol% to 6vol%) is presented in hornblende granodiorite porphyry as main mineral. Common accessory minerals are magnetite, apatite, and zircon. The granodioritic units are altered and next to magnetite-apatite veins hydrothermal alteration is

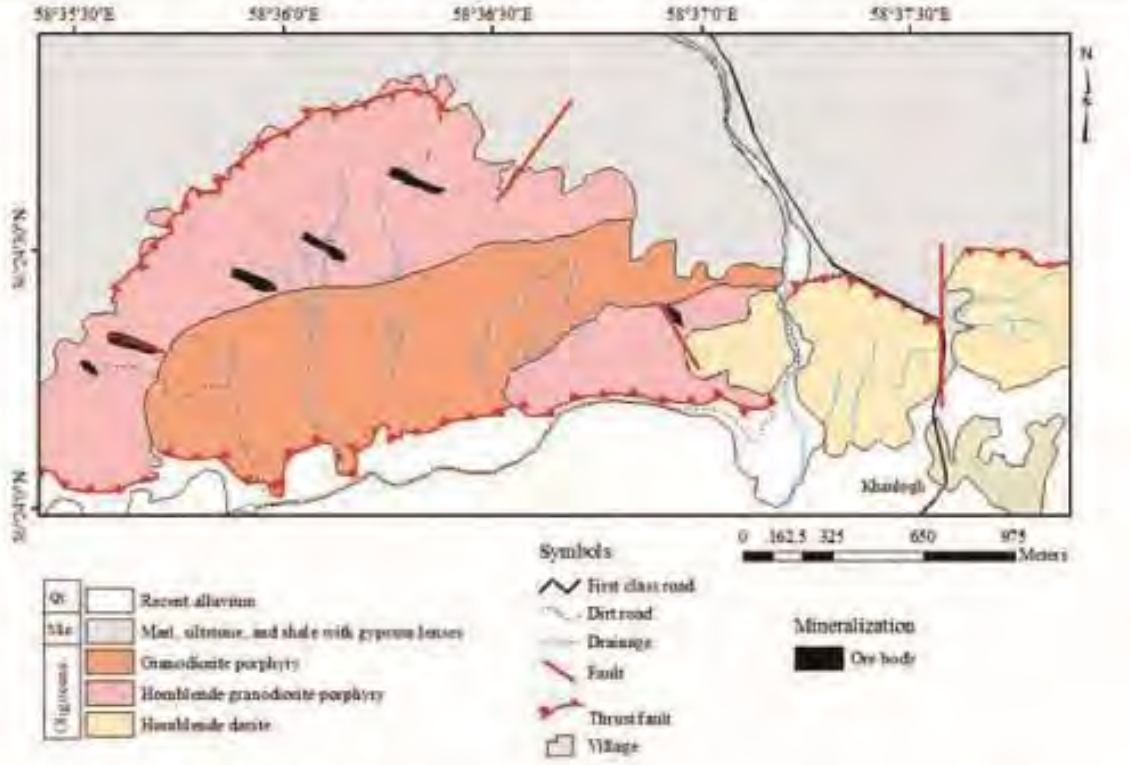

Fig. 2. Geologic map of the Khanlogh deposit.

intensified, and most of the igneous minerals are replaced with epidote, chlorite, calcite, quartz, illite, and montmorillonite.

The Miocene marl, siltstone, and red shale with gypsum lenses, which overlapped Oligocene igneous rocks, are 150–200 meter thick (Fig. 2). Ghaemi et al. (1998) suggested these rocks deposited in lagoon.

3 Analytical Methods

More than 200 polished slabs and thin sections were prepared from the intrusive rocks and ore samples collected from surface at the Khanlogh deposit for microscopic study. Twenty four whole-rock samples, apatite and magnetite crystals separated from deposit were analyzed for REE and trace elements. Trace elements and REE analysis was carried out at ACME Laboratory of Canada using ICP-MS techniques following lithium metaborate/tetraborate fusion after nitric acid digestion. Major elements of intrusive rock samples were analyzed at the Ferdowsi University of Mashhad, using a Philips PW1480 X-ray spectrometer. The geochemical results are listed in Tables 1 to 3.

4 Mineralization and Hydrothermal Alteration

Mineralization at Khanlogh occurs within the hornblende granodiorite porphyry (Fig. 2) and comprises several orebodies with similar alteration, mineralogy and texture. The orebodies are composed of six individual veins of iron oxide-apatite, which extend in an NW-SE direction, filling fractures and faults of the same trend along parallel fault zones (Fig. 3a). The magnetite-apatite veins range from 5 to 8 m in width, 20 to 150 m in length, and dip 25°–45° northeast. The mineralization is characterized by vein form with massive, brecciate, vein-veinlet, and open space filling textures. Veinlet texture, filling fractures of host rock, is a common texture of the deposit. The veinlets vary in thickness from a few millimeters to a few centimeters (Fig. 3b). The veinlets generally consist of magnetite, apatite, epidote, calcite, pyroxene, and quartz. There is open space filling texture, which occurs in the veinlet ores. Brecciated iron oxide ore is the second most dominant texture at the deposit. It consists of angular brecciated fragments of the host rock cemented by magnetite-apatite-calcite, which are observed in the fault zones (Fig. 3c). The massive ores consist of

predominantly magnetite with lesser amount apatite (Fig. 3d). Apatite locally is replaced by calcite and quartz.

The ore minerals at the Khanlogh deposit are dominated by magnetite and apatite with a few amounts of pyrite. The main gangue minerals include epidote, calcite, quartz, diopside, augite, and chlorite. Magnetite is the most dominant iron mineral in the deposit; although due to the effect of oxidation and supergene, magnetite have commonly been martitized along grain boundaries, fractures and octahedral cleavage faces. Magnetite crystals are commonly euhedral to subhedral and vary in size from a few millimeters to up to 7 centimeter (Fig. 4a). After magnetite, apatite is the second most dominant mineral, which occurs as euhedral crystals in creamy to light green color. Their size varies from 1 millimeter to 10 centimeter (Figs. 3d and 4b). Magnetite and apatite formed contemporaneously during the initial phase of mineralization. The main stage of mineralization (oxide mineralization) was followed by minor sulfide mineralization containing pyrite and chalcopyrite. Secondary minerals comprise hematite, goethite, and malachite. The mineralogy of the Khanlogh deposit is similar to that of the Kiruna-type IOA deposits.

The formation of Kiruna-type IOA deposits is associated with replacement and metasomatic alteration minerals of the host rocks, the most dominant among them being albite, K-feldspar, actinolite, sericite, biotite, muscovite, chlorite, epidote, and carbonate, and small amounts of tourmaline, barite, allanite, zircon, and fluorite (Daliran et al., 2007; Jami et al., 2007). According to Hitzman et al. (1992), in some alteration types at Kiruna district, a sort of zoning – from sodic to potassic (K-feldspar, sericite) to

Table 1 Chemical composition of the Khanlogh granodioritic rock

Sample No.	KH-44	KH-16	KH-25	KH-37	KH-40	KH-21	KH-4
Location	58°36'13" 36°24'32"	58°35'51" 36°24'24"	58°36'50" 36°24'21"	58°36'37" 36°24'22"	58°36'21" 36°24'31"	58°35'56" 36°24'28"	58°35'38" 36°24'21"
				wt%			
SiO_2	65.55	64.64	66.07	66.27	64.95	64.43	68.21
TiO_2	0.32	0.35	0.31	0.29	0.31	0.30	0.30
Al_2O_3	14.84	14.76	15.77	15.82	15.27	14.15	15.40
FeOt	3.91	3.18	2.71	3.36	3.76	3.71	3.15
MnO	0.08	0.05	0.04	0.07	0.04	0.06	0.05
MgO	3.54	3.40	2.18	1.75	3.28	3.96	0.88
CaO	4.5	4.68	4.32	4.71	4.02	4.55	4.34
Na_2O	3.16	4.51	5.28	3.65	3.84	2.70	5.24
K_2O	1.58	0.8	1.17	1.32	0.94	1.99	1.45
P_2O_5	0.13	0.14	0.04	0.12	0.13	0.12	0.05
L.O.I	2.23	3.29	1.94	2.54	3.32	3.91	0.79
Total	99.84	99.8	99.83	99.9	99.86	99.88	99.86
				ppm			
Ba	244	166	202	178	171	237	229
Co	9	7	5	6	8	9	4
Cs	0.7	0.3	1.2	3.6	1.1	0.6	2.2
Ga	14	14	13	14	13	13	12
Hf	2.2	2	2.1	1.9	2.3	2	2.3
Nb	4.6	4.3	3.5	3.4	3.8	3.5	3.1
Rb	28	12	22	37	22	41	41
Sr	346	424	381	372	315	361	499
Ta	0.4	0.3	0.3	0.2	0.3	0.2	0.2
Th	2.6	2.3	1.9	2.2	2.7	2.4	2.2
Zr	85	83	79	76	88	78	92
Y	9	7	6	7	7	9	8
La	10.2	9	5.8	8.6	9.9	11.5	6.6
Ce	18.5	16.5	11	15.8	18.3	19.7	11.7
Pr	2.01	1.77	1.37	1.68	1.98	2.09	1.51
Nd	7.3	7	5.8	6.4	7.4	7.7	6.9
Sm	1.51	1.41	1.28	1.33	1.56	1.42	1.66
Eu	0.42	0.48	0.41	0.46	0.43	0.49	0.47
Gd	1.43	1.31	1.20	1.37	1.34	1.45	1.57
Tb	0.25	0.21	0.21	0.22	0.22	0.23	0.25
Dy	1.46	1.19	1.18	1.12	1.22	1.34	1.40
Ho	0.29	0.24	0.24	0.26	0.27	0.29	0.26
Er	0.82	0.74	0.63	0.75	0.75	0.91	0.85
Tm	0.13	0.11	0.11	0.12	0.12	0.12	0.12
Yb	0.91	0.81	0.68	0.70	0.73	0.99	0.97
Lu	0.14	0.12	0.13	0.13	0.13	0.17	0.14
				Ratio			
K_2O/Na_2O	0.5	0.2	0.2	0.4	0.2	0.7	0.3
$(La/Yb)_N$	7.6	7.5	5.7	8.3	9.1	7.9	4.6
$(Co/Yb)_N$	5.3	5.3	4.2	5.8	6.5	5.2	3.1
Eu/Eu*	0.87	1.08	1.01	1.04	0.91	1.04	0.89

Table 2 Chemical composition of apatite in the Khanlogh deposit

Sample No.	A1	A2	A3	A4	A5	A6	A7	A8	A9
					ppm				
Ag	<0.02	<0.02	0.03	0.02	0.03	0.03	0.03	<0.02	<0.02
As	42	42	30	39	37	34	34	43	44
Ba	5	3	22	13	6	9	9	5	4
Bi	0.2	0.2	0.1	0.1	0.1	<0.04	<0.04	<0.04	<0.04
Co	0.2	<0.2	0.3	1.0	1.8	3.6	2.8	<0.2	0.4
Cr	11	11	17	21	18	23	24	13	15
Cu	1.7	1.4	2.5	3	3	3.1	3.6	1.1	3.6
Fe	2300	2100	2800	7400	7400	9600	10300	2100	4300
Li	1.0	0.9	1.1	1.0	1.0	1.0	1.0	1.1	0.7
Mo	0.1	0.2	0.3	1.9	0.3	0.4	0.8	0.1	0.6
Mn	297	297	312	309	389	440	355	291	322
Mg	800	800	800	1000	1100	1000	1000	800	800
Na	1340	1270	1590	1950	1740	1510	1890	1450	1480
Nb	0.05	0.05	0.06	0.05	0.09	0.11	0.23	0.16	0.14
Ni	2	0.8	1	39	7	8	9	2	6
Pb	2	1	4	6	2	3	5	2	2
Rb	0.3	0.1	0.2	0.3	0.2	0.2	0.2	0.2	0.2
Sb	0.2	0.1	0.8	0.4	0.3	0.3	0.3	0.2	0.2
Se	<0.3	0.8	<0.3	1.7	0.9	0.9	1.2	2.2	<0.3
Sr	567	559	613	778	737	628	696	577	576
Te	1.22	2.15	2.39	2.16	2.60	0.55	2.72	0.67	1.25
Th	233	235	216	276	123	109	196	244	240
Ti	490	520	520	600	590	500	560	510	520
U	5	5	6	8	8	7	7	5	5
V	71	70	76	88	108	114	114	68	72
Y	546	552	563	684	498	418	558	587	557
Zn	2	0.7	4	10	4	6	4	0.9	1
Zr	1	0.9	0.9	2	2	1	2	1	1
La	2000	2400	3000	2500	2670	2850	3100	2920	2670
Ce	3000	4200	3500	3200	4100	3650	4200	3620	3200
Pr	476.2	453.2	543.1	605.4	531.5	486.6	563.1	489.1	501.5
Nd	1845.7	1821.6	1958.1	2500	2420	1804.9	2300	1821.4	1882.3
Sm	247.1	237.8	265.6	309.7	265.2	227.3	270.6	253.2	260.1
Eu	25.7	25.9	21.8	26.4	25.6	21.3	25.2	26.8	26.3
Gd	182.9	171.7	194.5	219.4	189.3	148.7	193.1	169.9	176.2
Tb	21.8	20.0	23.1	28.9	21.7	19.6	24.5	22.5	21.9
Dy	120.0	111.7	125.7	146.7	106.6	98.4	131.2	115.6	118.1
Ho	22.0	21.1	23.7	26.6	19.6	18.8	23.3	21.3	21.3
Er	59.3	57.5	61.5	70.9	54.1	47.3	56.9	58.2	57.5
Tm	7.5	7.5	7.5	9.1	6.9	6.5	7.4	7.5	7.6
Yb	43.5	42.3	44.4	53.0	40.8	35.4	41.6	39.9	42.9
Lu	5.6	5.4	5.8	6.6	5.2	4.6	5.4	5.5	5.7
					Ratio				
$(La/Yb)_N$	31.0	38.3	45.6	31.8	44.1	54.3	50.2	49.3	42.0
$(Ce/Yb)_N$	17.8	25.7	20.4	15.6	26.0	26.7	26.1	23.5	19.3
Eu/Eu*	0.37	0.39	0.29	0.31	0.35	0.35	0.34	0.40	0.38
					Sum				
ΣREE	8057	9576	9775	9703	10457	9419	10942	9571	8991

sericitic and silicic – can be seen between the deeper and uppermost parts of the system. The country rocks of Khanlogh deposit exhibit marked hydrothermal alteration uppermost part of IOA-mineralized zone at surface. The alteration minerals include mainly epidote, calcite, diopside, augite, quartz, and chlorite. In the Khanlogh area, the alteration was confined mainly to the fractures and fault zones; the intensity of alteration decreases away from them. The alteration is manifested mainly by the replacement of hornblende and plagioclase phenocrysts by epidote, chlorite, calcite, and minor clay minerals in country rocks. Calcite is one of the most dominant alteration mineral, which occurs in three types, including fine-grained calcite associated with magnetite and apatite in vein and veinlets (Fig. 4c, e and f), coarse-grained calcite occurs rarely in open space filling texture, and later calcite veinlets cut the hypogene mineralization. Epidote associated with calcite is the most important gangue minerals at the Khanlogh deposit. There are large epidote grains around the ore veins (Fig. 4d). Diopside and augite are observed in veinlets around the orebody as single, radial or fan forms. The size of clinopyroxene grains reach to 1.5 centimeter (Fig. 4d and e). There are two different quartz generations at the deposit. First generation quartz occurred as considerably large subhedral to euhedral crystals within open space filling texture or quartz ± magnetite veinlets in host rock (Fig. 4f). Second generation quartz occurs as cryptocrystalline silica within cavities and

Table 3 Chemical composition of magnetite in the Khanlogh deposit

Sample No.	M1	M2	M3	M4	M5	M6	M7	M8
				ppm				
Ag	0.03	0.04	<0.02	<0.02	<0.02	0.04	0.03	0.04
Al	600	1000	900	600	1500	1100	1400	1600
As	29	7	39	36	25	17	40	54
Ba	3	3	5	4	6	4	5	9
Ca	200	300	2200	200	900	400	4400	600
Co	60	60	69	66	76	68	75	79
Cr	42	45	33	28	47	67	58	46
Cu	6	6	5	4	8	7	7	8
Ga	7	7	8	3	13	11	15	17
Hf	0.03	0.06	0.02	<0.02	0.05	0.02	<0.02	0.03
Li	0.3	0.3	0.8	0.5	1.1	0.3	0.9	1.0
Mo	6	10	57	43	11	17	15	29
Mn	261	287	473	339	664	366	439	692
Mg	500	600	1900	900	2700	1000	1000	1900
Na	70	60	50	50	60	80	70	110
Nb	2.51	1.58	3.97	2.31	4.57	3.05	3.27	4.19
Ni	354	353	451	350	475	437	460	525
P	50	40	820	110	280	260	1810	220
Pb	0.8	2	9	3	14	10	16	27
Rb	0.4	0.2	0.3	0.4	0.3	0.3	0.3	0.4
S	<40	60	<40	<40	<40	60	70	40
Sb	0.1	0.11	0.3	0.2	0.4	0.2	0.4	0.8
Sn	3.3	3.8	3.9	3.4	4.5	4.2	3.9	4.4
Sr	9	9	13	7	9	7	25	19
Ta	0.1	0.1	0.2	0.1	0.3	0.2	0.2	0.3
Th	0.4	0.2	1.8	0.6	0.9	0.7	4.5	1.4
Ti	2320	5580	2820	1070	8000	7230	5680	5340
U	0.1	<0.1	0.1	0.3	0.2	0.1	0.3	0.4
V	2265	2001	2754	1687	3183	3160	3230	3734
W	0.7	0.5	3.3	3.8	1.9	1.1	1.9	3.9
Y	0.9	0.4	4.1	1.2	2.6	1.7	9.2	3.0
Zn	55	56	62	87	63	59	59	84
Zr	4	5	3	3	6	5	3	3
La	1.0	0.9	14.5	1.1	5.8	4.5	30.5	4.2
Ce	2.07	1.76	28.63	2.34	12.11	8.88	62.77	8.42
Pr	0.2	0.2	3.1	0.4	1.3	1.1	6.9	1.0
Nd	1.1	1.0	11.0	1.3	4.2	3.6	21.7	3.5
Sm	0.2	<0.1	1.8	0.3	0.8	0.6	3.6	0.6
Eu	<0.1	<0.1	<0.1	<0.1	<0.1	<0.1	<0.1	<0.1
Gd	0.2	<0.1	1.4	0.2	0.7	0.4	2.4	0.7
Tb	<0.1	<0.1	<0.1	<0.1	<0.1	<0.1	<0.1	<0.1
Dy	0.2	<0.1	0.9	0.3	0.8	0.3	1.7	0.5
Ho	<0.1	<0.1	<0.1	<0.1	<0.1	<0.1	<0.1	<0.1
Er	0.1	<0.1	0.4	0.2	0.3	0.2	0.9	0.4
Tm	<0.1	<0.1	<0.1	<0.1	<0.1	<0.1	<0.1	<0.1
Yb	0.2	<0.1	0.5	0.2	0.3	0.2	0.6	0.4
Lu	<0.1	<0.1	<0.1	<0.1	<0.1	<0.1	<0.1	<0.1
				Ratio				
$(La/Yb)_N$	3.4	–	19.6	3.7	13.0	15.2	34.3	7.1
$(La/Sm)_N$	3.2	–	5.1	2.3	4.6	4.7	5.3	4.4
				Sum				
ΣREE	5	4	62	6	26	20	131	20

fractures of orebodies deposited in later stage of mineralization (Fig. 4b). Sodic and potassic alteration zones occur probably in deeper part of deposit, which needs to be confirmed by drilling.

5 Geochemistry

5.1 Host rock

Whole-rock major- and trace- [including rare earth elements (REEs)] element compositions of the Khanlogh granodioritic rocks are presented in Table 1. For geochemical classification of subvolcanic rocks, Na_2O + K_2O versus SiO_2 (Middlemost, 1985) compositional discrimination diagram is used (Fig. 5a). SiO_2 contents vary from 64.43wt% to 68.21wt%, K_2O from 0.8wt% to 2wt%, and K_2O/Na_2O ratio from 0.2 to 0.7 (Table 1). Therefore, the subvolcanic rocks are mostly medium-K calc-alkaline and less low-K. On the Alkali-FeOt-MgO (AFM) diagram (Irvine and Baragar, 1971), they plot in the calc-alkaline field (Fig. 5b). Utilizing the $Al_2O_3/(CaO + Na_2O + K_2O)$ versus $Al_2O_3/(Na_2O + K_2O)$ [A/CNK vs. A/NK] diagram (Shand, 1947), the granodioritic rocks plot in the metaluminous field and less peraluminous [A/CNK = 0.85–1.05] (Fig. 5c). Their alumina-saturation index

Fig. 3. (a) Vein-type mineralization within the hornblende granodiorite porphyry at the Khanlogh deposit: magnetite-apatite vein in altered host rock in the hanging wall; (b) magnetite veinlets fill the fractures of host rock; (c) brecciated fragments of the host rock cemented by magnetite and lesser amount apatite; (d) euhedral crystals of magnetite and apatite in massive texture.
Ap - apatite; Mag - magnetite from Whitney and Evans, 2010.

(ASI: molar Al_2O_3/ ($CaO + Na_2O + K_2O$)) remains below 1.1, which is the upper limit for I-type granitoids (Chappell and White, 2001) (Fig. 5c). The Khanlogh granodioritic rocks are enriched in incompatible elements (Table 1), especially, K, Rb, Ba, Sr, Cs, and Th, and depleted in high field strength (HFS) elements, such as Zr, Ti, Nb, Ta, and Y, which are indicative of arc-related magmatism (Thirlwall et al., 1994; Wilson, 2007). Based on Rb versus Y+Nb diagram, the rocks plot in the field of the volcanic arc granite in the diagram proposed by Pearce et al. (1984) (Fig. 5d). In the chondrite-normalized REE diagram (Boynton, 1984), all samples exhibit highly fractionated REEs, with moderately to slightly strong LREE enrichment ($9.1 \geq La_N/Yb_N \geq 4.6$ and $6.5 \geq Ce_N/Yb_N \geq 3.1$) (Table 1; Fig. 6a). The studied rocks also have Eu/Eu* [$Eu_{cn}/(Sm_{cn} + Gd_{cn})^{0.5}$] ratios from 0.87 to 1.08 (Table 1). All of the samples have a positive to slightly negative Eu anomaly (Fig. 6a).

The intrusions of Khanlogh area were generated by partial melting of mantle wedge, which is enriched by trace elements due to fluids derived subducted oceanic crust, during subduction of Sabzevar Neo-Tethyan oceanic lithosphere with continental margin of the Turan plate (Malekzadeh Shafaroudi et al., 2014).

5.2 Apatite

Apatite may concentrate a high proportion of REE, Sr, U, and Th (Ayers and Watson, 1993; Roeder et al., 1987). Variation in trace element concentrations within apatites is related to whole-rock parameters such as the SiO_2 activity, fO_2, total alkalis, the aluminium saturation index (ASI). The same parameters, and especially the relationship between fractionation and oxidation state, are critical to the development of magma-related porphyry and hydrothermal ore systems (Blevin and Chappell, 1995). Apatite contains significant amounts of REE substituting for Ca (Roeder et al., 1987; Rønsbo, 1989; Coulson and Chambers, 1996). This substitution has been shown previously to be coupled with substitution of Na^+ for Ca^{2+} and Si^{4+} for P^{5+} to achieve charge balance (Rønsbo, 1989).

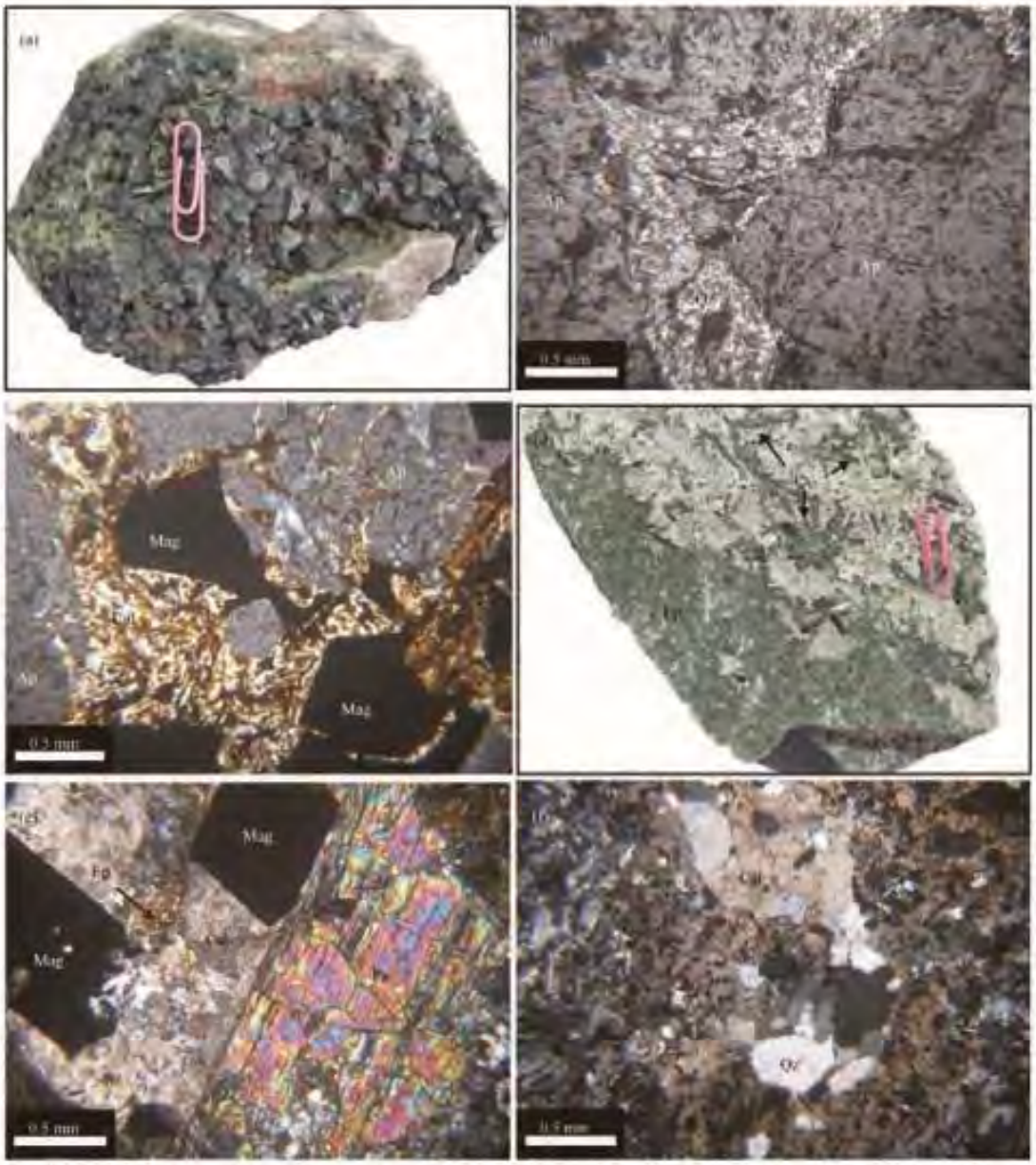

Fig. 4. (a) Hand specimen of euhedral magnetite crystals; (b) euhedral crystals of apatite and later cryptocrystalline quartz filling open space; (c) fine-grained calcite associated with euhedral crystals of magnetite and apatite in veinlet; (d) hand sample of epidote-calcite-pyroxene veinlet. Epidote and pyroxene are coarse grain and pyroxene occur as radial form; (e) coarse-grained diopside associated with euhedral magnetite crystals, epidote and fine-grained calcite; (f) fine-grained calcite and first generation quartz veinlet in host rock.
Ap - apatite; Mag - magnetite; Qz - quartz; Cal - calcite; Ep - epidote; Px - pyroxene from Whitney and Evans, 2010.

Chemical compositions of apatite grains are listed in Table 2. No significant difference in REE content is recognized among the apatite samples. In the chondrite-normalized REE diagram (Boynton, 1984), the all samples have similar patterns (Fig. 6b) and are characterized by highly fractionated REEs. The apatites of the Khanlogh ore contain about 8057–10942 ppm REE (Table 2). There is a strong fractionation with $(La/Yb)_N$=31–54.3 and $(Ce/Yb)_N$

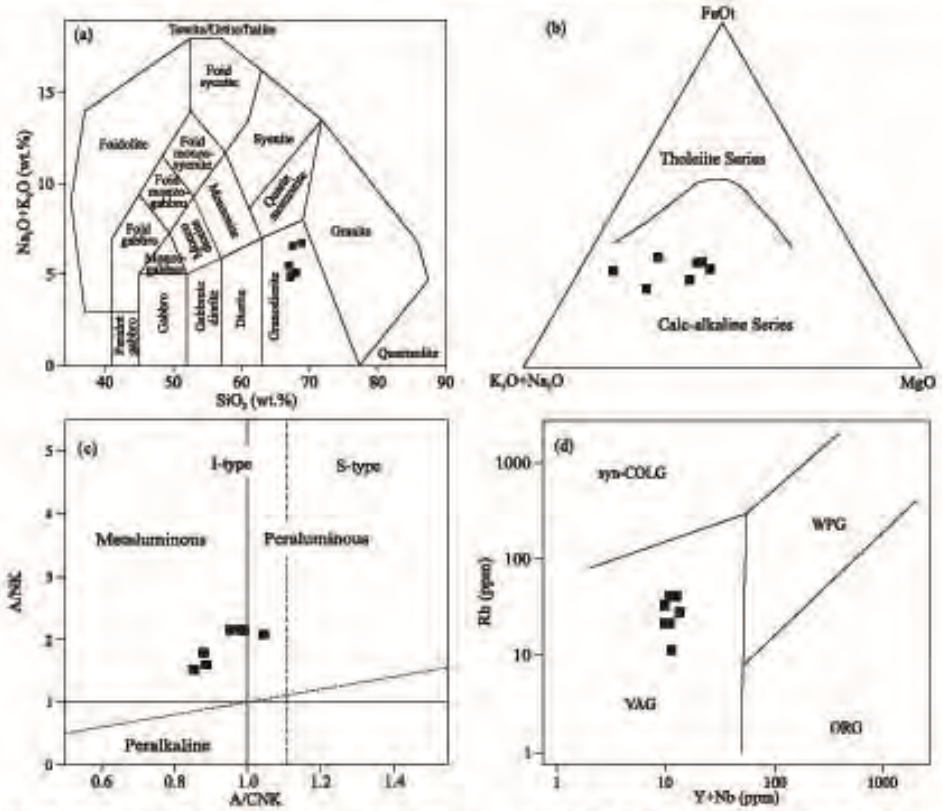

Fig. 5. Plot of host rock compositions on various diagrams: (a) $Na_2O + K_2O$ vs. SiO_2 compositional discrimination diagram (Middlemost, 1985) used for classification; (b) Alkali-FeOt-MgO (AFM) diagram (Irvine and Baragar, 1971); (c) A/CNK vs. A/NK diagram (Shand, 1947). The dashed line (A/CNK=1.1) divides the I-type field (A/CNK<1.1) from the S-type (A/CNK>1.1) field of Chappell and White (2001); (d) Tectonomagmatic discrimination diagram based on Rb vs. Nb+Y after Pearce et al. (1984).
WPG - within-plate granitoids; VAG - volcanic arc granitoids; ORG - ocean ridge granitoids; syn-COLG - syn-collisional granitoids.

=15.6–26.7 and negative Eu anomalies (Eu/Eu*=0.29 to 0.4) (Table 2 and Fig. 6b).

In addition, Sr contents vary from 559 to 778 ppm, Th from 109 to 276 ppm, and Y from 418 to 684 ppm, whereas U and Zr concentrations usually range from less than 8 and 2 ppm, respectively. Also, Fe and Mn values vary from 0.2wt% to 1wt% and 291 to 440 ppm, respectively (Table 2).

5.3 Magnetite

Magnetite can accommodate a variety of trace elements into their crystal structures. But only spinel elements such as Mg, Al, Ti, V, Cr, Mn, Co, Ni, Zn, and Ga are relatively enriched in magnetite because they can readily substitute Fe^{2+} or Fe^{3+} into magnetite spinel-type structure, (Deer et al., 1992). In addition, De Sitter et al. (1977) showed substitution of Ca^{2+} ions for the ferrous ion in the magnetite structure, which at most can contain 6.67wt% Ca^{2+}, corresponding to the composition $Ca_{0.5}Fe_{2.5}O_4$. Magnetites contain REE in small amounts replacing Ca^{2+}. The compositional variations of magnetite can be controlled by numerous factors including host rock geochemistry, mineral assemblage, degree of fluid-rock interaction, and physicochemical conditions during deposition (e.g. P, T, pH, fO_2, and fS_2) (Carew, 2004).

Chemical compositions of magnetite grains are listed in Table 3. Significant difference in REE content is recognized among the magnetite samples, but in the chondrite-normalized REE diagram (Boynton, 1984), the all samples have similar patterns (Fig. 6c). The magnetites of the Khanlogh ore contain about 4–131 ppm REE (Table 3). There is a weak to moderate fractionation with $(La/Yb)_N$ = 3.4–34.3 and $(La/Sm)_N$=2.3–5.3 and Eu value is below the detection limit (<0.1 ppm) (Table 3 and Fig. 6c).

In addition, Ti contents vary from 0.1wt% to 0.8wt%, S from <0.04wt% to 0.07wt%, and P from 0.004wt% to

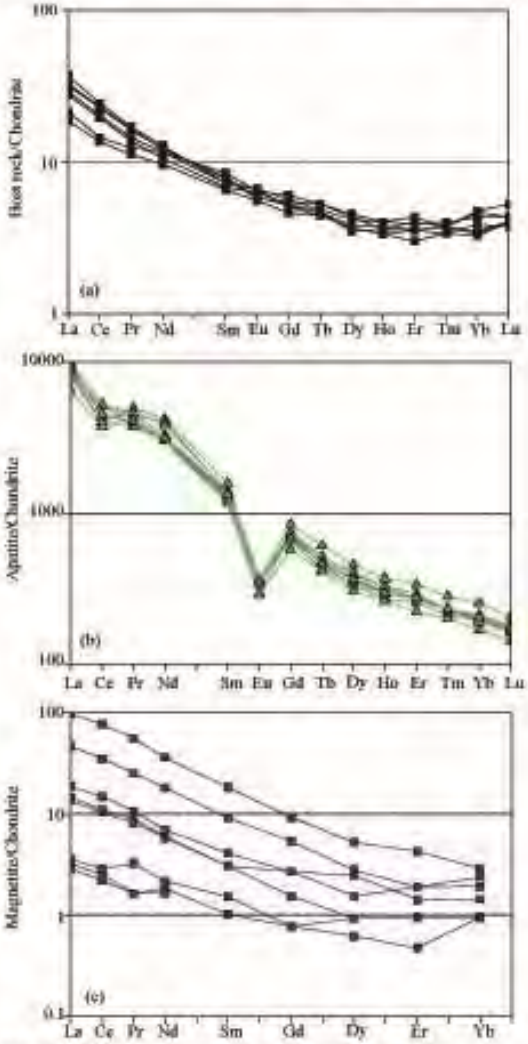

Fig. 6. (a) Chondrite-normalized REE patterns for the granodioritic rocks; (b) Chondrite-normalized REE patterns for the apatite samples; (c) Chondrite-normalized REE patterns for the magnetite samples from the Khanlogh deposit.
Normalizing values are from Boynton (1984).

0.2wt%. Therefore, the samples are low Ti-, S-, and P-magnetite. Al concentrations range from 600 to 1500 ppm, Mn from 261 to 692 ppm, Ni from 350 to 525 ppm, and V from 1687 to 3734 ppm. Also, Ca, Mg, and Cr values vary from 200 to 4400 ppm, 500 to 2700 ppm, and 28 to 67 ppm, respectively (Table 3).

6 Discussion

6.1 Comparison with the Kiruna-type apatite geochemistry

Apatites derived from different rock types and orebodies have distinctive absolute and relative abundances of many trace elements and REE. The scheme can be used for the recognition of apatites from specific rock types or styles of mineralization, so that the provenance of apatite grains in heavy mineral concentrates can be determined and used in geochemical exploration (Belousova et al., 2002).

Apatites from the Kiruna iron ores typically contain 2000–7000 ppm REE (Posht-e-Badam Block deposits apatites contain up to 2.5wt% REE; Daliran, 2002; Rahmani and Mokhtari, 2002; Mokhtari and Emami, 2008; and Tarom subzone from 9000 ppm to 1.2wt%; Nabatian et al., 2012) and are strongly LREE-enriched, with moderate to strong negative Eu anomalies (Frietsch, 1982; Frietsch and Perdahl, 1995). They contrast with the flat REE patterns of anorthosite-related apatites in 'Nelsonites' (apatite-magnetite bodies, e.g., Darling and Florence, 1995). In addition, the REE composition of the apatite in the magmatic iron ores is quite different from that in sedimentary apatite. The REE content in apatite from marine sediments and phosphorite is less than 1000 ppm or less than 100 times the chondrite-normalizaed values and show a Ce and Er depletion (Laajoki, 1975; Altschuler, 1980). The apatites of the magmatic magnetite- apatite ores of the Kiruna-type and the Khanlogh deposit show very similar in chondrite-normalized REE pattern (enrichment in LREE, a strong LREE/HREE fractionation, and negative Eu anomalies), however, the content of REE in the Khanlogh apatites varies from 8000 ppm to 1.1wt% and LREE/HREE fractionation is stronger (Fig. 7). These similar REE patterns indicate that the Khanlogh iron ore is magmatic. Also, Eu depletion indicates that associated magmas have undergone crystal fractionation with feldspar involved.

Plots of Sr versus Y and Mn allow the clearest definition of fields of apatite compositions for rock types and iron ores of contrasting composition. The Sr and Y contents of

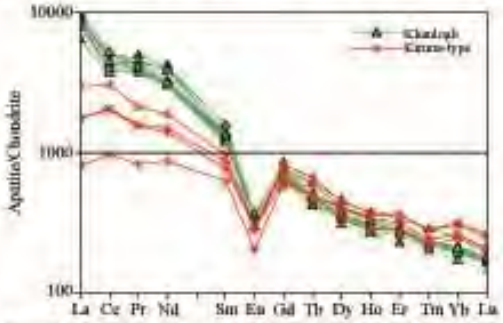

Fig. 7. Chondrite-normalized REE patterns of apatites from Kiruna-type iron ores and Khanlogh deposit.
Data for the Kiruna-type deposits after Frietsch and Perdahl (1995).

apatites vary widely and show a strong negative correlation, because Sr concentrations decrease with the degree of magmatic fractionation (from ultramafic rocks to mafic/intermediate rocks to granites and granite pegmatites), while Y contents increase. A plot of Sr against Mn concentrations shows weaker correlation than Sr against Y, probably because Mn contents in apatites depend not only on a degree of host rock fractionation, but also on its oxidation state (Belousova et al., 2002). The Khanlogh apatite values plotted on the Sr versus Mn and Y diagrams of Belousova et al. (2002) (Fig. 8a and b), which relates apatite chemistry to genetic association, support that the Khanlogh apatites are chemically very similar to those of other Kiruna-type deposits. Also, the amplitude of the negative Eu anomaly in the chondrite-normalized patterns generally increases with magmatic fractionation; it is lowest in the apatites from mantle-derived peridotites and carbonatites, and greatest in apatites from fractionated granitic rocks and pegmatites (Belousova et al., 2002). The apatites of Khanlogh deposit plot in the field of Kiruna-type iron ores with Eu/Eu* from 0.29 to 0.4 and Y from 418 to 684 ppm (Fig. 8c). In addition, the chondrite-normalized $(Ce/Yb)_N$ ratio is a direct measure of the steepness of the REE pattern, and thus of the enrichment of LREE relative to HREE. $(Ce/Yb)_N$, and hence the slope of the REE pattern, decreases from mafic/ultramafic rocks (including carbonatites) through mafic and intermediate rocks to granitoids and to highly fractionated rocks such as granite pegmatites, and this trend is not clearly related to total REE content (Belousova et al., 2002). In apatites of the Khanlogh iron ore, the $(Ce/Yb)_N$ contents vary from 15.6 to 26.7 and ΣREE from 8057 to 10942 ppm. These samples belong to the Kiruna-type deposits apatite on the $(Ce/Yb)_N$ versus ΣREE diagram of Belousova et al. (2002) (Fig. 8d).

6.2 Comparison with the Kiruna-type magnetite geochemistry

Magnetite can in corporate various amounts and assemblages of trace elements and REE during formation in various ore-forming environment, and hence the compositional variety can be used to fingerprint mineralization types and discriminate geochemical vectors (Carew et al., 2006; Singoyi et al., 2006; Rusk et al., 2009; Dupuis and Beaudoin, 2011; Zhang et al., 2011; Nadoll et al., 2012).

Magnetite of the different iron ores is relatively poor in REE (total amount approximately < 5 ppm) with a small fractionation or a depletion of LREE. The magnetite of the Kiruna iron ore type has the highest REE content (<100 ppm), with a marked LREE/HREE fractionation ($(La/Yb)_N$ <61). Typical is the fractionation of LREE ($(La/Sm)_N$ = 1–18), sloping down to a lower, flat level of HREE (Fig. 9a and b) (Frietsch and Perdahl, 1995). Comparison of chondrite-normalized patterns between the Kiruna-type different deposits and Khanlogh magnetites show very similar in some patterns (weak to moderate fractionation with $(La/Yb)_N$ <34 and $(La/Sm)_N$ <5) especially Kiirunavaara and Malmberget deposit in northern Sweden (Figs. 6c and 9). However, the REE content of Kiruna-type magnetites has high variations.

In addition, Dupuis and Beaudoin (2011) proposed that Al+Mn and Ni/(Cr+Mn) vs. Ti+V, diagrams can be used to discriminate among a wide variety of mineral deposits, including iron oxide-copper-gold (IOCG), banded iron formation (BIF), porphyry Cu, Fe-Cu skarn, Kiruna, and Fe-Ti-V mineralization (Fig. 10a and b). In the Khanlogh magnetites, the Ti+V (wt%) concentrations vary from 0.3wt% to 1.2wt% and Al+Mn from 0.09wt% to 0.2wt%. Therefore, the most samples plot in the field of Kiruna-type iron ores (Fig. 10a). Also, Ni/(Cr+Mn) ratios vary from 0.67 to 1.2 and the most magnetites are chemically very similar to those of other Kiruna-type deposits (Fig. 10b).

6.3 Ore genesis

In terms of mineralogy, texture, host rock lithology, alteration halos, and magnetite and apatite geochemistry, the Khanlogh deposits could be classified as Kiruna-type. The origin of the Kiruna-type deposits has been much debated and various formative processes have been suggested, ranging from magmatic origin due to liquid immiscibility (Frietsch, 1978; Kolker, 1982; Nyström and Henriquez, 1994) through exhalative-synsedimentary (Parak, 1991) to epigenetic-hydrothermal (Hilderband, 1986; Barton and Johnson, 1996; Mark and Foster, 2000; Sillitoe and Burrows, 2002; Zeng and Zhao, 2014). One of the most important genetic models is that they are considered as magmatic (segregation) deposits (Hitzman et al., 1992; Frietsch and Perdahl, 1995; Bookstrom, 1995). The magmatic genesis based on field observations is supported by the geochemical features of the main components of the ores. According to Frietsch and Perdahl (1995), the REE distribution in the apatite of different ores is related to the composition and source of enclosing host rocks. Strong LREE/HREE fractionation in apatites is connected with alkaline rocks and HREE>LREE distribution is connected with ultramafic rocs. Most of the apatite-bearing iron ores are associated with calc-alkaline magmas with a LREE/HREE fractionation varying from moderate to steep. Europium depletion results from Eu distribution into Ca-plagioclase in the early stage of crystal differentiation.

Comparison of chondrite-normalized REE patterns of apatite, magnetite, and granodioritic host rock indicates

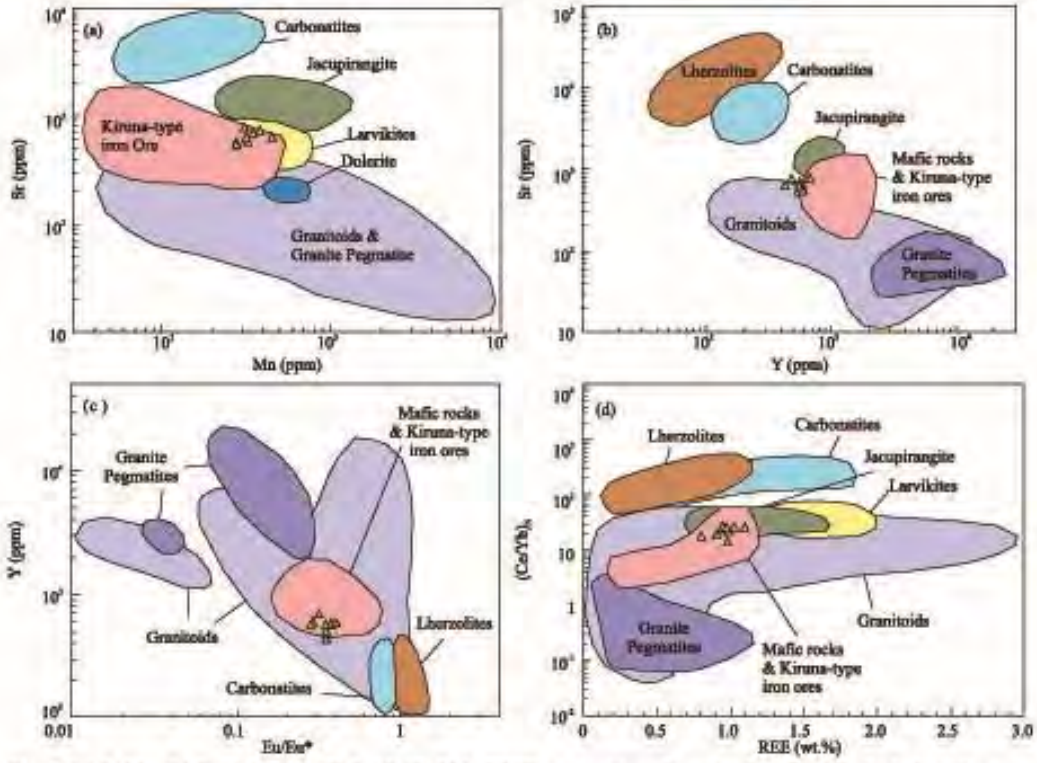

Fig. 8. (a) Sr-Mn; (b) Sr-Y; (c) Y-Eu/Eu*; (d) $(Ce/Yb)_N$-ΣREE composition of apatites from the Khanlogh deposit, compared to the reference fields of Belousova et al. (2002).

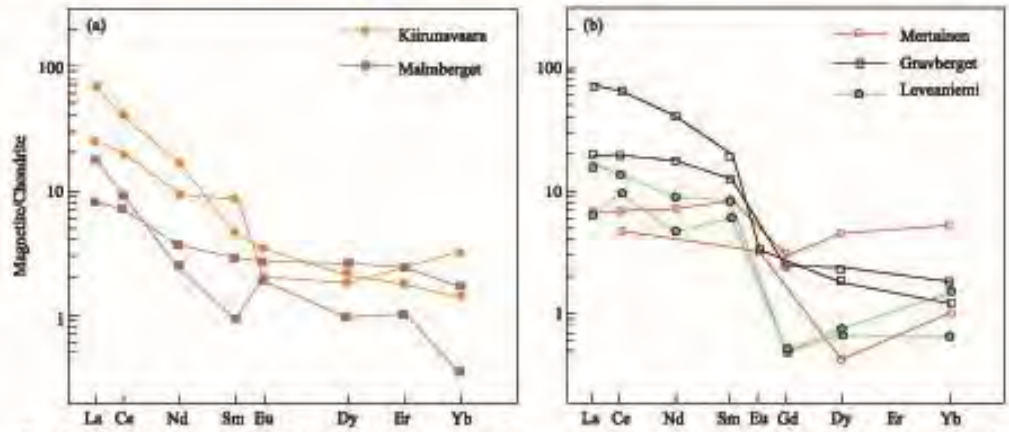

Fig. 9. Chondrite-normalized REE patterns for the magnetite samples from the Kiruna-type different deposits (Frietsch and Perdahl, 1995).

poor similar patterns in Eu anomalies, however moderate to steep LREE/HREE fractionation patterns are present in all of the samples (Fig. 6a to c). Field descriptions have determined the intensity of the alteration in the fractures and fault zones. The ore deposits in the study area were generated in these fractures, at varying widths and lengths (Fig. 11). At the rim of the ore deposits, the alteration zone is well formed. The width of this zone is related to two factors, the fault activity and the value of the ore deposits. Due to tectonic activity, it is not possible to separate the alteration zones clearly in some places. The occurrences of ore veins in the faults and fractures, suggest the

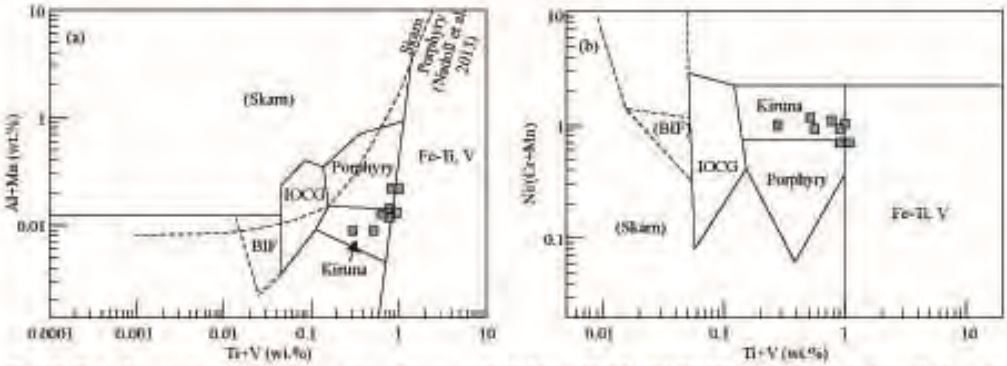

Fig. 10. Plot of magnetite compositions on two diagrams (a) Ti+V vs. Al+Mn; (b) Ti+V vs. Ni/(Cr+Mn) plot with deposit fields proposed by Dupuis and Beaudoin (2011)
Note: Values in weight percent.

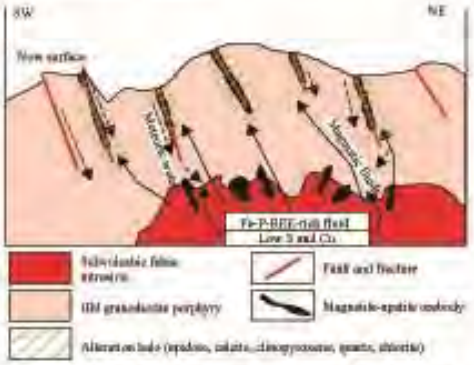

Fig. 11. Model for the formation of the Khanlogh deposit (see text for detail–not to scale).

granodioritic intrusions cannot be source rocks and there are no genetic relation between the iron deposits and these rocks. This claim is supported by the low exposure of orebodies at surface. It is likely that younger intrusion/ intrusions should be present in deeper part as source rock intruded the Oligocene granodiorite porphyry rocks (Fig. 11), which needs to be confirmed by drilling. The apatite chemistry from the Khanlogh deposit is characterized by enrichment in LREE and negative Eu anomalies could have resulted from the calc-alkaline feature of magmas (Frietsch and Perdahl, 1995). The generation of calc-alkaline magmas has been continued to Pliocene in Quchan-Sabzevar magmatic arc due to following oceanic lithosphere subduction beneath the Turan plat, NE Iran (Spies et al., 1984). Also, low Ti and V contents in magnetite indicate that this deposit was probably derived from magmatic-hydrothermal fluids related to felsic magmatism. In the Khanlogh deposit, the hydrothermal alteration halos correspond with uppermost part of IOA-mineralized zone and the mineral assemblages and the style of mineralization indicate a hydrothermal origin for the magnetite-apatite orebodies in this part of Iran.

Gandhi and Bell (1996) argued that processes of formation of IOCG and Kiruna-type deposits are magmatic fractionation and hydrothermal activity and the latter involves meteoric waters. The iron and other metals in these deposits are derived from a magmatic-hydrothermal source. In the Khanlogh deposit, magmatic-hydrothermal Fe-P-REE-rich fluids formed probably stockwork veins and massive mineralization at the top of the source magma at the early stages and then, the fractures and fault zones of country rocks were filled by hydrothermal ore-bearing solutions and caused the mineralization as vein-veinlet (Fig. 11). Together with oxide mineralization, hydrothermal fluids altered the granodioritic rocks and epidote, chlorite, calcite, quartz associated with large pyroxene formed around the orebody. The large pyroxene might have formed by the reaction of a Fe-Mg enriched hydrothermal fluid with the host rocks. The low content of sulfide mineralization and copper-bearing ore in the Khanlogh deposit indicate the ore fluid is S-Cu-poor. It is likely that at the final stage of mineralization, meteoric waters mixed with the magmatic fluid causing a decrease in its temperature (Fig. 11).

7 Conclusions

The Khanlogh magnetite-apatite deposit in the Quchan-Sabzevar magmatic arc is comparable with the Kiruna-type with which they share similarity in mineral chemistry evidence, setting, form of orebodies, and alteration zoning. The orebodies are genetically related to calc-alkaline felsic magmatism generated within the subduction zone between Sabzevar Neo-Tethyan oceanic lithosphere and the continental margin of the Turan plate.

The geological studies, mineralogy, geochemical

characteristics, and hydrothermal alteration of the Khanlogh deposit and host rock indicate that this magnetite deposit is not the result of silica-iron oxide immiscibility, but are related to post magmatic hydrothermal activity similar to Cenozoic Kiruna-type deposits in northwest Iran. The fluids that originated during the post magmatic events were responsible for removing the iron from the host rocks, after which these fluids migrated to the cracks and fractures of the host rock. With respect to the Khanlogh deposit is a first Kiruna-type IOA occurrence that was introduced within the Cenozoic Quchan-Sabzevar magmatic arc, NE Iran, and regional detailed exploration was proposed for IOA and IOCG deposits in this part of Iran.

8 Acknowledgments

The present study is based on the first author's MS.c thesis at Ferdowsi University of Mashhad, Mashhad, Iran. Field studies and some laboratory costs were funded by the Ferdowsi University of Mashhad Research Grant Council. We are very grateful to Dr. Degan Shu and anonymous reviewers for their constructive suggestions on the manuscript.

Manuscript received Aug. 11, 2014
accepted Jan. 10, 2015
edited by Liu Xinzhu and Fei Hongcai

References

Altschuler, Z.S., 1980. The geochemistry of trace elements in marine phosphorites, 1: Characteristic, abundance and enrichment. Society of Economist, Paleontologist and Mineralogist, Special Publication, 29: 19–30.

Ayers, J.C., and Watson, E.B., 1993. Apatite/fluid partitioning of rare earth elements and strontium: experimental results at 1.0 GPa and 1000°C and application to models of fluid-rock interaction. *Chemical Geol.*, 110: 299–314.

Azizi, H., Mehrabi, B., and Akbarpour, A., 2009. Genesis of Tertiary magnetite-apatite deposits, southeast of Zanjan, Iran. *Resource Geol.*, 59(4): 330–341.

Barton, M.D., and Johnson, D.A., 1996. Evaporitic-source model for igneous-related Fe oxide-(REE-u-Au-U) mineralization. *Geology*, 24: 259–262.

Bauman, A., Spies, O., and Lensch, G., 1983. Strontium isotopic composition of post-ophiolithic tertiary volcanics between Kashmar, Sabzevar and Quchan NE Iran. In: Almassi, A. (ed.), *Geodynamic Project (Geotraverse) in Iran*. Tehran: Geological Survey of Iran. 267–276.

Beaudoin, G., and Dupuis, C., 2009. Iron-oxide trace element fingerprinting of mineral deposit types. In: Corriveau, L., and Mumin, A.H. (ed.), *Exploration for Iron Oxide Copper-gold Deposits: Canada and Global Analogues*. GAC Short Course Notes, 107–121.

Belousova, E.A., Griffin, W.L., O'Reilly, S.Y., and Fisher, N.I., 2002. Apatite as an indicator mineral for mineral exploration: trace-element compositions and their relationship to host rock type. *J. Geochem. Exploration*, 76: 45–69.

Berzina, A., 2012. Platinum-group element geochemistry of magnetite from porphyry-Cu-Mo deposits and their host rocks (Siberia, Russia). *Acta Geologica Sinica* (English Edition), 86 (1): 106–117.

Blevin, P.L., and Chappell, B.W., 1995. Chemistry, origin and evolution of mineralized granites in the Lachlan Fold Belt, Australia: the metallogeny of I- and S-type granites. *Economic Geol.*, 90: 1604–1619.

Bookstrom, A.A., 1995, Magmatic features of iron ores of the Kiruna type in Chile and Sweden: Ore textures and magnetite geochemistry: A discussion. *Economic Geol.*, 90: 469–473.

Boynton, W.V., 1984. Cosmochemistry of the rare earth elements, Meteorite studies. In: Henderson, P. (ed.), *Rare Earth Element Geochemistry*. Amesterdam: Elsevier, 115–1522.

Bonyadi, Z., Davidson, G.J., Mehrabi, B., Meffre, S., and Ghazban, F., 2011. Significance of apatite REE depletion and monazite inclusions in the brecciated Se-Chahun iron oxide-apatite deposit, Bafq district, Iran: Insights from paragenesis and geochemistry. *Chemical Geol.*, 281: 253–269.

Carew, M.J., 2004. Controls on Cu-Au mineralization and Fe oxide metasomatism in the Eastern Fold Belt, NW Queensland, Australia. Queensland: James Cook University (Ph. D thesis), 213–277.

Carew, M.J., Mark, G., Oliver, N.H.S., and Pearson, N., 2006. Trace element geochemistry of magnetite and pyrite in Fe oxide (+/–Cu-Au) mineralized systems: Insights into the geochemistry of ore-forming fluid. *Geochim. Cosmochim. Acta*, 70(18): A83–A83.

Chappell, B.W., and White, A.J.R., 2001. Two contrasting granite types, 25 years later. *Australian J. Earth Sci.*, 48: 489–500.

Coulson, I.M., and Chambers, A.D., 1996. Patterns of zonation in rare-earth-bearing minerals in nepheline syenites of the North Qôroq Center, South Greenland. Canadian Mineral., 34: 1163–1178.

Daliran, F., 2002. Kiruna-type iron oxide-apatite ores and apatites of the Bafq district, Iran, with an emphasis on the REE geochemistry of their apatites. In: Porter, T.M. (ed.), *Hydrothermal Iron Oxide Copper-gold and Related Deposits*. Adelaide: PGC Publishing, 303–320.

Darling, R.S., and Florence, F.P., 1995. Apatite light rare earth element chemistry of the Port Leyden Nelsonite, Adirondack Highlands, New York: implications for the origin of Nelsonite in anorthosite suite rocks. *Economic Geol.*, 90: 964–968.

Daliran, F., Stosch, H.G., and Williams, P., 2007. Multistage metasomatism and mineralization at hydrothermal Fe oxide-REE apatite deposits and "apatites" of the Bafq district, central east Iran. In: Stanely, C.J. et al. (eds.), *Digging Deeper*, Proceeding of 9th Biennial SGA Meeting Dublin, 1501–1504.

Daliran, F., Stosch, H.G., and Williams, P., 2010. Lower Cambrian iron oxide-apatite-REE (U) deposits of the Bafq district, east- Central Iran. In: Corriveau, L., and Mumin, H. (ed.), *Exploring for Iron-oxide Copper-gold Deposits: Canada and Global Analogues*. Québec: Geological Association of Canada and Geological Survey of Canada, 143–155.

Dawson, J.B., and Hinton, R.W., 2003. Trace-element content and partitioning in calcite, dolomite and apatite in carbonatite, Phalaborwa, South Africa. *Mineral Magazine*, 67(5): 921–

930.

Dawson, J.B., Steele, I.M., Smith, J.V., and Rivers, M.L., 1996. Minor and trace element chemistry of carbonates, apatites and magnetites in some African carbonatites. *Mineral Magazine*, 60: 415–425.

Deer, W.A., Howie, R.A., and Zussman, J., 1992. *An Introduction to the Rock-forming Minerals* (2nd ed). New York: Longman, Harlow, Wiley, 696.

De Sitter, J., Govaert, A., De Grave, E., Chamaere, D., and Robrecht, G., 1977. Mossbauer study of Ca^{2+}-containing magnetites. *Physicochem. Status Solidification*, 43(a): 619–624.

Dupuis, C., and Beaudoin, G., 2011. Discriminate diagrams for iron oxide trace element fingerprinting of mineral deposit types. Mineralium Deposita, 46(3): 1–17.

Fatehi, H., 2014. Geology, mineralization, and geochemistry of Jalambadan deposit, NW Sabzevar. Mashhad: Ferdowsi University of Mashhad (MS. c thesis), 240.

Forster, H., and Jafarzadeh, A., 1994. The Bafq mining district in Central Iran: a highly mineralized Infracambrian volcanic field. Economic Geol., 89: 1667–1721.

Frietsch, R., 1978. On the magmatic origin of iron ores of the Kiruna type. *Economic Geol.*, 73: 478–485.

Frietsch, R., 1982. On the chemical composition of the ore breccia at Luossavaara, northern Sweden. *Mineral. Deposita*, 17: 239–243.

Frietsch, R., and Perdahl, J.A., 1995. Rare earth elements in apatite and magnetite in Kiruna-type iron ores and some other iron ore types. *Ore Geology Rev.*, 9: 489–510.

Gandhi, S.S., and Bell, R.T., 1996. Kiruna/Olympic Dam-type iron, copper, uranium, gold, silver. In: Eckstrand, O.R., Sinclair, W.D.., and Thorpe, R.I. (ed.), *Geology of Canadian Mineral Deposit Types*. Québec: Geological Survey of Canada, 513–522.

Gelcich, S., Davis, D.W., and Spooner, E.T.C., 2005. Testing the apatite-magnetite geochronometer: U-Pb and $^{40}Ar/^{39}Ar$ geochronology of plutonic rocks, massive magnetite–apatite tabular bodies, and IOCG mineralization in northern Chile. *Geochim. Cosmochim. Acta*, 69: 3367–3384.

Ghaemi, F., Ghaemi, F., and Hosseini, K., 1998. Geological Map of Nyshabour 1:100,000. Tehran: Geological Survey of Iran.

Gholami, S., 2009. Geology, mineralization, geochemistry, and magnetometry of Shotorsang iron deposit, NE Sabzevar. Mashhad: Ferdowsi University of Mashhad (MS. c thesis), 174.

Groves, D.I., Bierlein, F.P., Meinert, L.D., and Hitzman, M.W., 2010. Iron Oxide Copper-Gold (IOCG) deposits through Earth history: implications for origin, lithospheric setting, and distinction from other epigenetic iron oxide deposits. *Economic Geol.*, 105: 641–654.

Hildebrand, R.S., 1986. Kiruna-type deposits: their origin and relationship to intermediate subvolcanic plutons in the Great Bear Magmatic Zone, northwest Canada. *Economic Geol.*, 81: 640–659.

Hitzman, M.W., 2000. Iron oxide-Cu-Au deposits: what, where, when and why. In: Porter, T.M. (ed.), *Hydrothermal Iron Oxide Copper-gold and Related Deposits. A Global Perspective*. Adelaide: Australian Mineral Foundation, 9–25.

Hitzman, M.W., Oreskes, N., and Einaudi, M.T., 1992. Geological characteristics and tectonic setting of Proterozoic iron oxide (Cu-U-Au-LREE) deposits. *Precambrian Res.*, 58: 241–287.

Hughes, J.M., Cameron, M., and Mariano, A.N., 1991. Rare earth element ordering and structural variations in natural rare earth bearing apatites. *American Mineral.*, 76: 1165–1173.

Irvine, T.N., and Baragar, W.R.A., 1971. A guide to the chemical classification of the common volcanic rocks. *Canadian J. Earth Sci.*, 8: 523–548.

Jami, M., 2005. Geology, geochemistry and evolution of the Esfordi phosphate-iron deposit, Bafq area, Central Iran. University of South Wales (Ph. D thesis), 403 p.

Jami, M., Dunlop, A.C., and Cohen, D.R., 2007. Fluid inclusion and stable isotope study of the Esfordi apatite-magnetite deposit, Central Iran. *Economic Geol.*, 102, 1111–1128.

Karimpour, M.H. Malekzadeh Shafaroudi, A., Esfandiarpour, A., and Mohammadnejad, H., 2012. Neyshabour Torquise mine: the first Cu-Au-U-LREE IOCG type in Iran. Iranian *J. Economic Geol.* 1(3): 193–216 (in Persian with English abstract).

Kolker, A., 1982. Mineralogy and geochemistry of Fe-Ti oxide and apatite (nelsonite) deposits and evaluation of the liquid immiscibility hypothesis. *Economic Geol.*, 77: 1146–1158.

Laajoki, J.M., 1975. Rare earth elements in Precambrian iron formations in Vayrylankyla, south Puolanka area, Finland. *Bull. Geol. Soc. Finland*, 47: 93–107.

Malekzadeh Shafaroudi, A., Karimpour, M.H., and Zarei, A., 2014. Petrology, geochemistry, and tectonic setting of Tertiary volcanic and intrusive rocks in north of Shahr-e-Firouzeh, NE Iran. *J. Petrol.* (under review) (in Persian with English abstract).

Mark, G., and Foster, D.R.W., 2000. Magmatic albite-actinolite-apatite rich rocks from the Cloncurry district, Northwest Queensland, *Australian Lithos*, 51: 223–245.

Middlemost, E.A.K., 1985. *Magmas and Magmatic Rocks*. London: Longman Publication Co., 221–226.

Mokhtari, M.A.A., and Emami, M.H., 2008. REE patterns and REE mineralization in apatite-magnetite deposits of Bafq-Saghand District (Central Iran). *Geosciences* (special issue), 17(1): 161–168.

Mokhtari, M.A.A., Hosseinzadeh, G., and Emami, M.H., 2013. Genesis of iron-apatite ores in Posht-e-Badam Block (Central Iran) using REE geochemistry. *J. Earth System Sci.* 122(3): 795–807.

Nabatian., G., and Ghaderi, M., 2013. Oxygen isotope and fluid inclusion study of the Sorkhe-Dizaj iron oxide-apatite deposit, NW Iran. *Intl. Geol. Rev.* 55(4): 397–410.

Nabatian, G., Ghaderi, M., Daliran, F., and Rashidnejad-Omran, N., 2012. Sorkhe-Dizaj Iron Oxide-Apatite Ore Deposit in the Cenozoic Alborz-Azarbaijan Magmatic Belt, NW Iran. *Resource Geol.*, 63(1): 42–56.

Nadoll, P., Mauk, J.L., Hayes, T.S., Koenig, A.E., and Box, S.E., 2012. Geochemistry of magnetite from hydrothermal ore deposits and host rocks of the Mesoproterozoic Belt Supergroup, United States. *Economic Geol.*, 107(6): 1275–1292.

Nyström, J.O., and Henriquez, F., 1994. Magmatic features of iron ores of the Kiruna type in Chile and Sweden: ore textures and magnetite geochemistry. *Economic Geol.*, 89: 820–839.

O'Reilly, S.Y., and Griffin, W.L., 2002. Apatite in the mantle: implications for metasomatic processes and high heat production in Phanerozoic mantle. *Lithos*, 53: 217–232.

Rahmani, Sh., and Mokhtari, M.A.A., 2002. Exploration of

metallic rare elements. *Geol. Survey Iran*, 365 (in Persian).

Roeder, P.L., MacArthur, D., Xin-Pei, Ma., Palmer, G.R., and Mariano, A.N., 1987. Cathodoluminescence and microprobe study of rare earth elements in apatite. *American Mineral.*, 72: 801–811.

Rønsbo, J.G., 1989. Coupled substitutions involving REEs and Na and Si in apatites in alkaline rocks from the Ilimaussaq intrusion, South Greenland, and the petrological implications. *American Mineral.*, 74: 896–901.

Rusk, B.G., Oliver, N.H.S., Zhang, D., Brown, A., Lilly, R., and Jungmann, D., 2009. Compositions of magnetite and sulfides from barren and mineralized IOCG deposits in the eastern succession of the Mt Isa Inlier. Townsville: Australia Society for Geology Applied to Mineral Deposits, 10th Bi-ennial SGA Meeting, 656–658.

Parak, T., 1991. Volcanic sedimentary rock-related metallogenesis in the Kiruna-Skellefte belt of northern Sweden. *Economic Geology Monograph*, 8: 20–50.

Pearce, J.A., Harris, N.W., and Tindle, A.G., 1984. Trace element discrimination diagrams for the tectonic interpretation of granitic rocks. *J. Petrol.*, 25: 956–983.

Sahandi, M.R., Soheily, M., Sadeghi, M., Delavar, S.T., and Jafari Rad, A., 2002. Geological Map of Iran, 1:1,000,000. Tehran: Geological Survey of Iran.

Shand, S.J., 1947. *Eruptive Rocks*. New York: D. Van Nostrand Company, 488.

Sillitoe, R.H., and Burrows, D.R., 2002. New field evidence bearing on the origin of the El Laco magnetite deposit, Northern Chile. *Economic Geol.*, 97: 1101–1109.

Singoyi, B., Danyushevsky, L., Davidson, G.J., Large, R., and Zaw, K., 2006. Determination of trace elements in magnetites from hydrothermal deposits using the LA ICP-MS technique. SEG Keystone Conference. Denver, USA: CD-ROM.

Spies O., Lensch G., and Mihem A., 1984. Petrology and geochemistry of the post-ophiolitic Tertiary volcanic between Sabzevar and Quchan, NE Iran. *J. Geol. Paleontol.*, 168(2/3): 389–408.

Taylor, R.P., and McLennan, S.M., 1985. *The Continental Crust: Its Composition and Evolution*. Blackwell: Oxford, 312.

Thirlwall, M.F., Smith, T.E., Graham, A.M., Theodorou, N., Hollings, P., Davidson, J.P., and Arculus, R.J., 1994. High field strength elements anomalies in arc lavs: source or process? *J. Petrol.*, 35: 819–838.

Torab, F.M., and Lehmann, B., 2007. Magnetite-apatite deposits of the Bafq district, Central Iran: apatite geochemistry and monazite geochronology. *Mineral Magazine*, 71, 347–363.

Watson, E.B., and Green, T.H., 1981. Apatite/liquid partition coefficients for the rare-earth elements and strontium. *Earth Planet. Sci. Lett.*, 56: 405–421.

Whitney, D.L., and Evans, B.W., 2010. Abbreviations for names of rock-forming minerals. *American Mineral.*, 95: 185–187.

Williams, P.J., 2010. Classifying IOCG deposits. In: Corriveau, L., and Mumin, H. (ed.), *Exploring for Iron-oxide Copper Gold Deposits: Canada and Global Analogues*. Québec: Geological Association of Canada and Geological Survey of Canada, 11–19.

Williams, P.J., Barton, M.D., Fontboté, L., de Haller, A., Mark, G., Oliver, N.H.S., and Marschik, R., 2005. Iron-oxide-copper gold deposits: geology, space-time distribution, and possible modes of origin. Society of Economic Geologists, Economic Geology 100th Anniversary Volume, Denver, 371–405.

Wilson, M., 2007. *Igneous Petrogenesis*. Berlin: Springer, Verlag, 466.

Huang Xiaowen, Qi Liang and Meng Yumiao, 2014. Trace element geochemistry of magnetite from the Fe(-Cu) deposits in the Hami region, eastern Tianshan orogenic belt, NW China. *Acta Geologica Sinica* (English Edition) 88 (1): 176–195.

Zarei, A., Malekzadeh Shafaroudi, A., and Karimpour, M.H., 2014. Magnetite-apatite Khanlogh deposit, northwest of Neyshabour: Mineralogy, texture and structure, alteration, and determination of model. Iranian J. Mineral. Crystallogr. (in press) (in Persian with English abstract).

Zhang, D., Rusk, B., Oliver, N., and Dai, T., 2011. Trace element geochemistry of magnetite from the Ernest Henry IOCG deposit, Australia. 11th biennial meeting SGA 2011-Let s talk ore deposits. Antofagasta, Chile, 85.

ZENG Liping and ZHAO Xinfu, 2014. Apatite Mineralogy and Chemistry of the Taocun Magnetite-Apatite Deposit in Ningwu Volcanic Basin: Implications for Ore Genesis of IOA Deposits. Acta Geologica Sinica (English Edition), 88(supp. 2): 1493–1494.

About the first author

Arezo Zarei, Male; born in Mashhad in 1987. He graduated from department of Geology, Ferdowsi University of Mashhad, Iran as a Bs.c in 2011, now he is Ms.c student in Ferdowsi University of Mashhad, Iran. His current interests include ore genesis of IOCG deposits and petrogenesis of magmatism related to mineralization.

E-mail: zare-i@stu.um.ac.ir.